

Neptune Second Harmonic Generation Autocorrelator

Joel England

UCLA Dept. of Physics and Astronomy

Particle Beam Physics Laboratory

April 7, 2005

■ I. Introduction

This document provides detailed information on the basic theoretical knowledge required to understand the operational principles of the Second Harmonic Generation Autocorrelator used for measuring the pulse length of the infrared drive laser at the Neptune Laboratory. This autocorrelator was originally assembled by Kari Sanders and Sergei Tochitsky ca. 2000-2001. Some information about its operation may be found in Kari Sanders' master's thesis. In short, the autocorrelator operates by splitting the infrared (1064nm) pulse produced by the Neptune regenerative amplifier and grating compressor and then crossing the two split pulses inside of a nonlinear KDP crystal, via a Type I "ooe" interaction, to produce noncollinear second harmonic frequency upconversion to green (532 nm). The intensity of the green as a function of the delay between the two split pulses produces the autocorrelation of the pulse, which can be used to extract the pulse length and (to some extent) the time structure of the pulse. The theory of autocorrelation will not be discussed in this document.

■ II. Basics of Nonlinear Optics

■ Maxwell Equations with Generalized Polarization

In their most general form, Maxwell's Equations read

$$\begin{aligned}\nabla \cdot \mathbf{E} &= 4\pi\rho ; \\ \nabla \times \mathbf{E} &= -\frac{1}{c} \frac{\partial \mathbf{B}}{\partial t} ; \\ \nabla \cdot \mathbf{B} &= 0 \\ \nabla \times \mathbf{B} &= \frac{1}{c} \frac{\partial \mathbf{E}}{\partial t} + \frac{4\pi}{c} \mathbf{J} ;\end{aligned}\tag{1}$$

with the current and charge densities being connected by the continuity equation,

$$\nabla \cdot \mathbf{J} + \frac{\partial \rho}{\partial t} = 0\tag{2}$$

We may separate the current density into a DC component \mathbf{J}_0 and a time-dependent component \mathbf{J}_t such that $\mathbf{J}(\mathbf{r}, t) = \mathbf{J}_0(\mathbf{r}) + \mathbf{J}_t(\mathbf{r}, t)$. We can then suppose that \mathbf{J}_t is the time derivative of some function \mathbb{P} , so that we write

$$\mathbf{J} = \mathbf{J}_0 + \frac{\partial \mathbb{P}}{\partial t} ; \quad \rho = \rho_0 - \nabla \cdot \mathbb{P}\tag{3}$$

The second relation follows by substitution of the first into (2) and defining $\rho_0 \equiv \nabla \cdot \mathbf{J}_0$. Then, (1) may be cast into the form

$$\begin{aligned}
\nabla \cdot \mathbf{D} &= 4\pi\rho_0; \\
\nabla \times \mathbf{E} &= -\frac{1}{c} \frac{\partial \mathbf{B}}{\partial t}; \\
\nabla \cdot \mathbf{B} &= 0 \\
\nabla \times \mathbf{B} &= \frac{1}{c} \frac{\partial \mathbf{D}}{\partial t} + \frac{4\pi}{c} \mathbf{J}_0;
\end{aligned} \tag{4}$$

where we have defined a generalized displacement field:

$$\mathbf{D} = \mathbf{E} + 4\pi\mathbf{P} \tag{5}$$

In general, \mathbf{P} is a function of both \mathbf{E} and \mathbf{B} , (i.e. $\mathbf{P} = \mathbf{P}[\mathbf{E}, \mathbf{B}]$) since it contains the electric and magnetic dipole responses which are both intimately connected to the fields. If we consider the case where there is no magnetic material present, then it becomes a function only of \mathbf{E} . For sufficiently weak electric fields, the functional $\mathbf{P}[\mathbf{E}]$ can then be expanded in powers of the components of \mathbf{E} :

$$\mathbf{P} = \sum_{n=1}^{\infty} \tilde{\mathbf{F}}^{(n)}[\mathbf{E}] \tag{6}$$

where $\tilde{\mathbf{F}}^{(n)}$ in component form read

$$\begin{aligned}
\tilde{F}_i^{(1)}[\mathbf{E}] &= \int \tilde{X}_{ij}^{(1)}(\mathbf{r} - \mathbf{r}_1, t - t_1) E_j(\mathbf{r}_1, t_1) d^3 r_1 dt_1; \\
\tilde{F}_i^{(2)}[\mathbf{E}] &= \int \tilde{X}_{ijk}^{(2)}(\mathbf{r} - \mathbf{r}_1, t - t_1; \mathbf{r} - \mathbf{r}_2, t - t_2) E_j(\mathbf{r}_1, t_1) E_k(\mathbf{r}_2, t_2) d^3 r_1 dt_1 d^3 r_2 dt_2; \\
&\dots
\end{aligned} \tag{7}$$

Here $\tilde{X}^{(n)}$ is a tensor of rank $n + 1$ whose components represent the expansion coefficients. There is also an implied summation on repeated indices. If \mathbf{E} is a superposition of plane waves:

$$\mathbf{E}(\mathbf{r}, t) = \sum_i \mathbf{E}^{(i)}; \quad \text{where } \mathbf{E}^{(i)}(\mathbf{k}_i, \omega_i) = \hat{\mathbf{E}}^{(i)} e^{i(\mathbf{k}_i \cdot \mathbf{r} - \omega_i t)} \tag{8}$$

then the Fourier transforms of (5) are

$$\begin{aligned}
\mathbf{F}^{(1)} &= \mathbf{X}^{(1)} : \mathbf{E}^{(1)}; \\
\mathbf{F}^{(2)} &= \mathbf{X}^{(2)} : \mathbf{E}^{(1)} \mathbf{E}^{(2)}; \\
\mathbf{F}^{(3)} &= \mathbf{X}^{(3)} : \mathbf{E}^{(1)} \mathbf{E}^{(2)} \mathbf{E}^{(3)}; \\
&\dots
\end{aligned} \tag{9}$$

where, $\mathbf{X}^{(n)}$ is the generalized susceptibility tensor of rank $n + 1$. It is given explicitly by the Fourier transform of the coefficients in (5):

$$\mathbf{X}^{(n)} = \int \tilde{\mathbf{X}}^{(n)}(\mathbf{q} - \mathbf{q}', \boldsymbol{\tau} - \boldsymbol{\tau}') e^{-i[\mathbf{K}(\mathbf{q} - \mathbf{q}') - \mathbf{W}(\boldsymbol{\tau} - \boldsymbol{\tau}')] } d^3 q' d^n \boldsymbol{\tau}' \tag{10}$$

where for compactness we define the composite vectors

$$\begin{aligned}
\mathbf{q} &= (\mathbf{r}, \mathbf{r}, \dots, \mathbf{r}); \quad \mathbf{q}' = (\mathbf{r}_1, \mathbf{r}_2, \dots, \mathbf{r}_n); \\
\boldsymbol{\tau} &= (t, t, \dots, t); \quad \boldsymbol{\tau}' = (t_1, t_2, \dots, t); \\
\mathbf{K} &= (\mathbf{k}_1, \mathbf{k}_2, \dots, \mathbf{k}_n); \quad \mathbf{W} = (\omega_1, \omega_2, \dots, \omega_n)
\end{aligned} \tag{11}$$

■ Connection to Maxwell's Equations in Linear Media

We begin by taking the time-dependent part of the current and charge distributions to be due to the usual electric and magnetic dipole contributions \mathbf{P} and \mathbf{M} . These are related by expanding the distributions in multipoles to dipole order, giving us

$$\mathbf{J} = \mathbf{J}_0 + \frac{\partial \mathbf{P}}{\partial t} + c \nabla \times \mathbf{M} \quad ; \quad \rho = \rho_0 - \nabla \cdot \mathbf{P} \quad (12)$$

Hence, according to (2) the generalized polarization function \mathbb{P} is given by

$$\frac{\partial \mathbb{P}}{\partial t} = \frac{\partial \mathbf{P}}{\partial t} + c \nabla \times \mathbf{M} \quad (13)$$

and the generalized displacement field is thus

$$\mathbb{D} = \mathbf{E} + 4\pi \mathbf{P} + c \int \nabla \times \mathbf{M} dt \quad (14)$$

Then, setting

$$\mathbf{D} = \mathbf{E} + 4\pi \mathbf{P} \quad ; \quad \mathbf{H} = \mathbf{B} - \mathbf{M} \quad (15)$$

Equations (3) become

$$\begin{aligned} \nabla \cdot \mathbf{D} &= 4\pi \rho_0 ; \\ \nabla \times \mathbf{E} &= -\frac{1}{c} \frac{\partial \mathbf{B}}{\partial t} ; \\ \nabla \cdot \mathbf{B} &= 0 \\ \nabla \times \mathbf{H} &= \frac{1}{c} \frac{\partial \mathbf{D}}{\partial t} + \frac{4\pi}{c} \mathbf{J}_0 ; \end{aligned} \quad (16)$$

These are the usual form of Maxwell's equations in macroscopic media. By definition a linear medium is one in which the derived fields are linear functions of the components of the primary fields, which we may write in the form

$$\mathbf{D} = \hat{\epsilon} \cdot \mathbf{E} \quad ; \quad \mathbf{H} = \hat{\mu}^{-1} \cdot \mathbf{B} \quad (17)$$

where $\hat{\epsilon}$ and $\hat{\mu}$ are the dielectric and magnetic permeability tensors. Now, via (14) and (16) we have that

$$\mathbf{P} = \chi \cdot \mathbf{E} \quad , \quad \text{where} \quad \chi \equiv \frac{1}{4\pi} (\hat{\epsilon} - \mathbf{I}) \quad (18)$$

The matrix χ is called the electric susceptibility tensor. This equation has the form of equation (8). We therefore conclude that the linear susceptibility tensor χ is equal to the lowest order generalized susceptibility tensor $\mathbf{X}^{(1)}$. We can therefore rewrite (17) in the following equivalent form as expressed in the generalized notation

$$\mathbf{P} = \mathbf{X}^{(1)} : \mathbf{E} = \begin{pmatrix} \chi_{11} & \chi_{12} & \chi_{13} \\ \chi_{21} & \chi_{22} & \chi_{23} \\ \chi_{31} & \chi_{32} & \chi_{33} \end{pmatrix} \cdot \begin{pmatrix} E_x \\ E_y \\ E_z \end{pmatrix} \quad (19)$$

In the case where the medium is isotropic, the response is the same in all directions and the susceptibility tensor is a diagonal matrix with $\chi_{11} = \chi_{22} = \chi_{33} = \chi$. In this case the equations above simplify to the usual linear relations for isotropic media:

$$\mathbf{D} = \epsilon \mathbf{E} \quad ; \quad \mathbf{P} = \chi \mathbf{E} \quad ; \quad \epsilon = 4\pi\chi + 1 \quad (20)$$

■ Second Order Phase Matching Conditions

To second order, the generalized polarization in component form reads

$$\mathbb{P}_i = X_{ij}^{(1)} E_j + X_{ijk}^{(2)} E_j E_k \quad (21)$$

The first order contribution is given by (18). Due to the presence of the second-order interaction, two waves of different wavenumbers \mathbf{k}_1 and \mathbf{k}_2 can interact within the crystal to produce a third outgoing wave whose wavevector \mathbf{k}_3 is either their sum or difference. These phenomena we call respectively *sum phase matching* and *difference phase matching*:

$$\mathbf{k}_3 = \begin{cases} \mathbf{k}_1 + \mathbf{k}_2 & ; \quad \text{sum phase matching} \\ \mathbf{k}_2 - \mathbf{k}_1 & ; \quad \text{difference phase matching} \end{cases} \quad (22)$$

By additionally requiring that the output *frequency* be either twice the input frequencies or their difference, we produce the following subsets of the two conditions above, called respectively *second harmonic generation* and *difference frequency generation*:

$$\begin{cases} \omega_3 = 2\omega_1 = 2\omega_2 & \Rightarrow & 2n_3 \hat{\mathbf{k}}_3 = n_1 \hat{\mathbf{k}}_1 + n_2 \hat{\mathbf{k}}_2 & ; \quad \text{SHG} \\ \omega_3 = \omega_2 - \omega_1 & \Rightarrow & (\omega_2 - \omega_1) n_3 \hat{\mathbf{k}}_3 = n_2 \omega_2 \hat{\mathbf{k}}_2 - n_1 \omega_1 \hat{\mathbf{k}}_1 & ; \quad \text{DFG} \end{cases} \quad (23)$$

After obtaining expressions for n_i for the material in question, these matching conditions may be applied to solve for the relative intersection angle (called the *phase matching angle*) of the incident waves with the optical axis, which will produce the desired type of output.

■ III. Nonlinear Optics in Uniaxial Crystals

■ The Indices of Refraction

In a uniaxial crystal, there is a special direction called the *optical axis*, which we will take to be $\hat{\mathbf{z}}$. The optical axis and the wave-vector \mathbf{k} define a plane called the *principal plane*. Waves polarized perpendicular to the principal plane are called *ordinary* waves, while those whose polarization lies within the plane are called *extraordinary* waves. The indices of refraction N_e and N_o are different for these two polarizations. They may be written [Dmitriev, *Handbook of Nonlinear Optical Crystals*, p. 7]

$$\begin{aligned} N_o &= n_o = \text{constant}; \\ N_e(\theta) &= n_o \left\{ \frac{(1 + \tan^2 \theta)}{1 + (n_o/n_e)^2 \tan^2 \theta} \right\}^{1/2} \end{aligned} \quad (24)$$

where $n_e = N_e(\theta = \pi/2)$ and θ is the angle between the optical axis and the direction of propagation:

$$\hat{\mathbf{z}} \cdot \hat{\mathbf{k}} = \cos \theta \quad (25)$$

The relative magnitudes of n_o and n_e define two different classes of uniaxial crystals:

$$\begin{aligned} n_e < n_o & \quad \text{"negative crystal"} \\ n_e > n_o & \quad \text{"positive crystal"} \end{aligned} \quad (26)$$

■ The Collinear Phase Matching Conditions

Based upon our above classification of the propagating waves as ordinary or extraordinary, we can divide the possible cases of second order 3-wave interactions into two classes:

$$\begin{aligned} \text{Type I} & : \text{ both input waves are ordinary or extraordinary} \\ \text{Type II} & : \text{ input waves have orthogonal polarization} \end{aligned} \quad (27)$$

Among these two groups we have respectively the following possibilities:

$$\begin{aligned} \text{Type I SHG} & : \text{ eeo, ooe} \\ \text{Type II SHG} & : \text{ oee, oeo} \end{aligned} \quad (28)$$

where "eeo" for example means that the input waves are extraordinary and the output wave is ordinary. The designations of (25) further subdivide Type II according to whether the crystal is positive or negative:

Output	Type I		Type II	
	Positive	Negative	Positive	Negative
<i>o</i> :	eeo	–	eeo	oeo
<i>e</i> :	–	ooe	oeo	oee

Applying the phase matching conditions with the results of the previous section we obtain the following expressions for the *collinear* matching angle $\tan^2 \theta$ for each of the cases represented in the table above:

Output	Type I		Type II	
	Positive	Negative	Positive	Negative
<i>o</i> :	$(1 - U)/(U - S)$	–	$(1 - T)/(T - Z)$	$(1 - V)/(V - Y)$
<i>e</i> :	–	$(1 - U)/(W - 1)$	$(1 - U)/(W - R)$	$(1 - U)/(W - Q)$

where

$$\begin{aligned} U &= (A + B)^2 / C^2; \quad W = (A + B)^2 / F^2; \quad R = (A + B)^2 / (D + B)^2; \\ Q &= (A + B)^2 / (A + E)^2; \quad S = (A + B)^2 / (D + E)^2; \quad V = B^2 / (C - A)^2; \\ Y &= B^2 / E^2; \quad T = A^2 / (C - B)^2; \quad Z = A^2 / D^2; \\ A &= n_{o1} / \lambda_1; \quad B = n_{o2} / \lambda_2; \quad C = n_{o3} / \lambda_3; \\ D &= n_{e1} / \lambda_1; \quad E = n_{e2} / \lambda_2; \quad F = n_{e3} / \lambda_3; \end{aligned} \quad (31)$$

Note that for Type I interactions, "eeo" interactions occur only in Positive crystals and "ooe" interactions occur only in Negative crystals. This is because otherwise the relative signs of n_o and n_e lead to phase-matching equations which have no real-valued solutions.

■ Derivation of the Collinear "oeo" Phase Matching Angle

Let us calculate the noncollinear phase matching relationship for two ordinary waves incident with frequencies ω_1 and ω_2 at a crossing angle 2α . We take the principal plane to be the x-z plane with the optical axis along z. Then, we can write

$$k_1 = N_o(\omega_1) \frac{\omega_1}{c}; \quad k_2 = N_o(\omega_2) \frac{\omega_2}{c}; \quad k_3 = N_e(\omega_3, \theta) \frac{\omega_3}{c} \quad (32)$$

where N_o and N_e are given by (23). Then, requiring $k_3 = k_1 + k_2$ we obtain the relation

$$N_o(\omega_1) \omega_1 + N_o(\omega_2) \omega_2 = N_e(\omega_3, \theta) \omega_3 \quad (33)$$

or

$$n_{o1} \omega_1 + n_{o2} \omega_2 = n_{o3} \omega_3 \left\{ \frac{(1 + \tan^2 \theta)}{1 + (n_{o3}/n_{e3})^2 \tan^2 \theta} \right\}^{1/2} \quad (34)$$

Note that the wavelength inside the crystal and the wavelength outside the crystal are different. Namely, $\lambda_{\text{ext}} = n \lambda_{\text{int}}$. Since is more convenient to refer to the external wavelength, we will denote $\omega_i = 2\pi c/\lambda_i$ where $i = 1, 2, 3$. Then, (34) reads

$$\frac{n_{o1}}{\lambda_1} + \frac{n_{o2}}{\lambda_2} = \frac{n_{o3}}{\lambda_3} \left\{ \frac{(1 + \tan^2 \theta)}{1 + (n_{o3}/n_{e3})^2 \tan^2 \theta} \right\}^{1/2} \quad (35)$$

or in terms of the quantities defined by (31) this reads

$$A + B = C \left\{ \frac{(1 + \tan^2 \theta)}{1 + (C/F)^2 \tan^2 \theta} \right\}^{1/2} \quad (36)$$

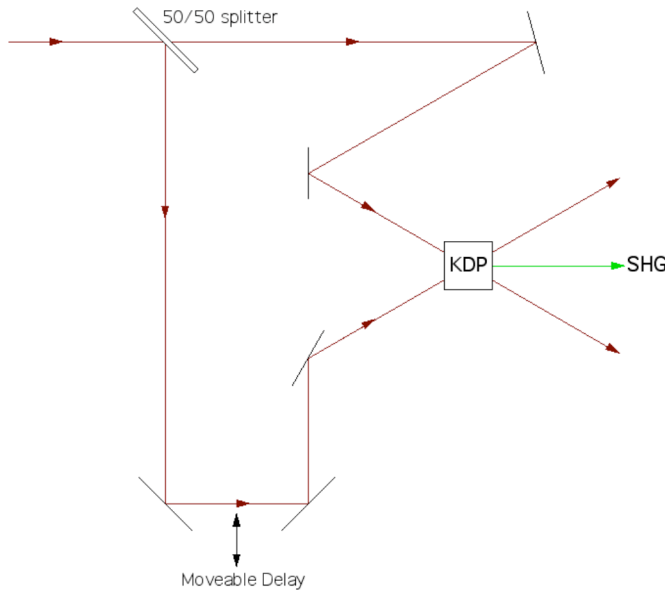
Solving this for $\tan^2 \theta$ we obtain the expected result from table (30).

$$\tan^2 \theta = \frac{1 - (A+B)^2/C^2}{(A+B)^2/F^2 - 1} = \frac{1 - U}{W - 1} \quad (37)$$

■ IV. The Neptune SHG Autocorrelator

■ Introduction

The autocorrelator for the Neptune Laboratory is a homemade device constructed originally for K. Sander's EE master's thesis. The operating principle is as follows. The amplified IR laser pulse (1.064 μm) from the Regen, after compression by the gratings, is split into two beams and then recombined in a KDP crystal with a crossing angle ψ external to the crystal that produces an internal crossing angle α that corresponds to the proper matching angle for second-harmonic generation. A moveable delay on one leg permits the two pulses to be overlapped within the crystal. A cartoon diagram of the setup is shown below.



Because the interaction occurs only over the transverse distance corresponding to the intersection region of the two pulses in space, the width of the resultant green (532 nm) SHG pulse is related to the pulse length of the input beams. By observing the width of the SHG light with a CCD camera, one can then deduce the pulse length of the laser pulse in a single shot. This requires, however, that the input IR pulse be made transversely very large. If the input pulse is small then the device can still be operated as a multishot device. The autocorrelation trace can then be produced by measuring

■ **KDP Crystals**

The name of the nonlinear crystal KDP is short for Potassium Dihydrogen Phosphate or KH_2PO_4 . It is a negative, uniaxial crystal. It can support second harmonic interactions of type "oeo" and third harmonic interactions of type "eoe". Note that Type I "eoo" interactions are forbidden for negative crystals. Consequently, for SHG in KDP, the crossed input beams must have *ordinary* polarizations. The wavelength dependences of the indices of refraction for KDP at 25°C are given by [Dmitriev, *Handbook of Nonlinear Optical Crystals*, p. 54]

$$\begin{aligned}
 n_o^2(\lambda) &= 2.259276 + \frac{0.01008956}{\lambda^2 - 0.012942625} + \frac{13.00522 \lambda^2}{\lambda^2 - 400} ; \\
 n_e^2(\lambda) &= 2.132668 + \frac{0.008637494}{\lambda^2 - 0.012281043} + \frac{3.2279924 \lambda^2}{\lambda^2 - 400} ;
 \end{aligned}
 \tag{38}$$

where λ is in μm . So, for SHG with an input wavelength of $\lambda = 1.064 \mu\text{m}$ we obtain the following values:

Symbol	$\lambda(\mu\text{m})$	Eq. (38)
$n_{o,2\omega}$	0.532	1.5124
$n_{e,2\omega}$	0.532	1.4705
$n_{o,\omega}$	1.064	1.4938
$n_{e,\omega}$	1.064	1.4599

(39)

■ The Noncollinear "ooe" Phase Matching Angle for SHG

Let us calculate the noncollinear phase matching relationship for SHG with two ordinary waves incident with frequency ω at an angle 2α . We take the principal plane to be the x-z plane with the optical axis along z. Then, we can write

$$\mathbf{k}_1 = N_o(\omega) \frac{\omega}{c} \hat{\mathbf{k}}_1 ; \quad \mathbf{k}_2 = N_o(\omega) \frac{\omega}{c} \hat{\mathbf{k}}_2 ; \quad \mathbf{k}_3 = N_e(2\omega, \theta) \frac{2\omega}{c} \hat{\mathbf{k}}_3 \quad (40)$$

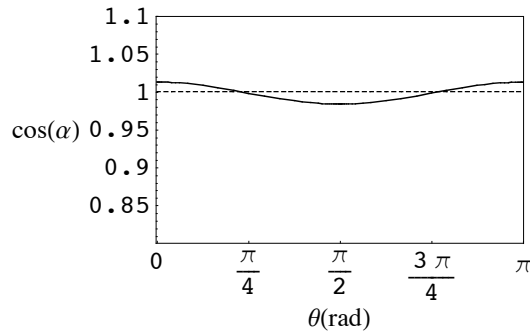
where N_o and N_e are given by (23) and

$$\begin{aligned} \hat{\mathbf{k}}_1 &= \cos(\theta + \alpha) \hat{\mathbf{z}} + \sin(\theta + \alpha) \hat{\mathbf{x}} ; \\ \hat{\mathbf{k}}_2 &= \cos(\theta - \alpha) \hat{\mathbf{z}} + \sin(\theta - \alpha) \hat{\mathbf{x}} ; \\ \hat{\mathbf{k}}_3 &= \cos\theta \hat{\mathbf{z}} + \sin\theta \hat{\mathbf{x}} ; \end{aligned} \quad (41)$$

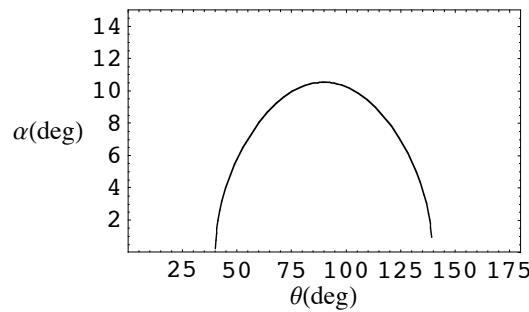
Then, requiring $\mathbf{k}_3 = \mathbf{k}_1 + \mathbf{k}_2$ we obtain the relation

$$\cos\alpha = \frac{n_{o,2\omega}}{n_{o,\omega}} \left\{ \frac{(1 + \tan^2\theta)}{1 + [n_{o,2\omega}/n_{e,2\omega}]^2 \tan^2\theta} \right\}^{1/2} \quad (42)$$

This relationship tells us that if we wish to generate an output wave that propagates at an angle θ from the optical axis, then the two input waves must propagate at the angles $\theta \pm \alpha$ where α is given by (42). The indices of refraction are given in table (39). With these values we obtain the following plot of $\cos\alpha$ vs. θ :



Note that real-valued solutions for α occur only within the region below the dotted line. Plotting the inverse cosine of the above graph within this region we obtain the following solutions for α :



The peak occurs at $\theta = 90^\circ$. We find from (40) that at this matching angle, the intersection angle of the initial wavevectors is given by

$$\alpha = \arccos \frac{n_{e,2\omega}}{n_{o,\omega}} = 10.1^\circ \quad [\text{for } 90^\circ \text{ phase - matching}] \quad (43)$$

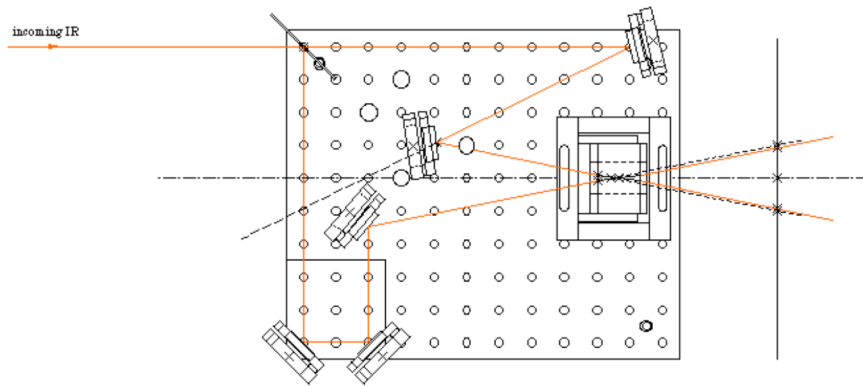
The values of θ corresponding to $\alpha = 0$ represent the collinear phase-matching solutions:

$$\theta = \arctan \frac{n_{e,2\omega}}{n_{o,2\omega}} \left\{ \frac{n_{o,\omega}^2 - n_{o,2\omega}^2}{n_{e,2\omega}^2 - n_{o,\omega}^2} \right\}^{1/2} = 41.2^\circ, 138.8^\circ \quad [\text{collinear phase - matching}] \quad (44)$$

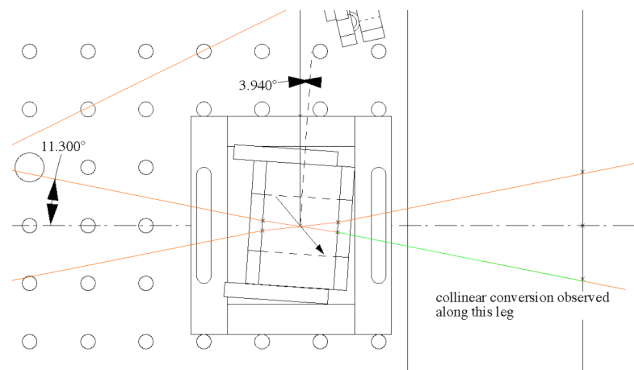
The smaller value matches the prediction of equation (37). The larger value simply corresponds to a reversal of the direction of propagation through the crystal. Note that in [K. Sanders, *Up-Conversion of THz Amplitude-Modulated CO₂ Laser Pulses Using Nonlinear Crystals* (PhD. Thesis), p. 52], it says that the measured bisected internal intersection angle for two incident 1.064 μm pulses was $\alpha=7.6^\circ$. This value of α corresponds on the plot above to $\theta=58.18^\circ$. It was determined empirically and theoretically (see below) that this angle quoted in the Sander's thesis is incorrect. The correct crossing angle is calculated in the following section.

■ Crossing Angles for the Neptune SSA

The apparatus for the Neptune SSA is shown in the following diagram:

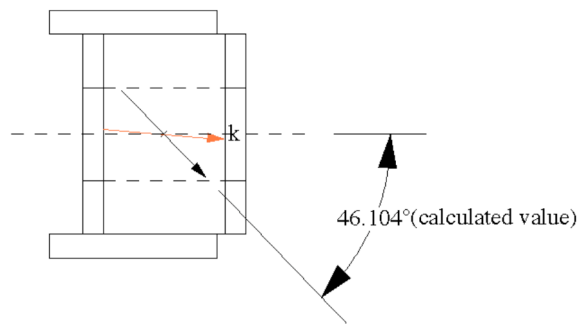


The label on the KDP crystal indicates that it is an INRAD KDP "D" crystal. The "D" designation, according to the INRAD website, indicates the cut. For type D this is indicated as corresponding to an optical axis at an angle of 46.6° from the geometrical longitudinal axis of the crystal in the horizontal plane. The collinear phase matching angle was observed experimentally for an incidence angle of 11.3° with a $1.064\mu\text{m}$ wavelength input beam. In order to get collinear green at 532nm the crystal had to be rotated by 3.94° . Using equation (44) then gives a crystal cut orientation of 46.1° , when the refraction of the beam inside the crystal is taken into account. This arrangement is shown in the following figure:



A blowup of the crystal with the measured orientation of the optical axis and the k-vector direction for collinear matching is shown below.

inrad D-type: optical axis cut at 46.6° according to web site



Our goal now is to calculate the correct orientation of the KDP apparatus to get *noncollinear* phase matching. For the sake of simplicity, we would like the cut angle to coincide with the angle θ of the exiting wave-vector, so that the SHG beam will exit at right angles to the crystal surface and we therefore will not have to rotate the crystal at all. We therefore set $\theta = \theta_{\text{cut}} = 46.6^\circ$. At this value, equation (42) predicts that $\alpha = 4.16^\circ$. In order to get an internal crossing angle of this magnitude, we therefore need the input beams to have an external bisected crossing angle of $\phi_e = 6.2^\circ$. In summary, the correct angles for the KDP in the Neptune SSA are as follows:

Angle	Value	Description
α	4.16°	external crossing (bisected)
ϕ_e	6.2°	internal crossing (bisected)
θ	46.6°	crystal cut angle

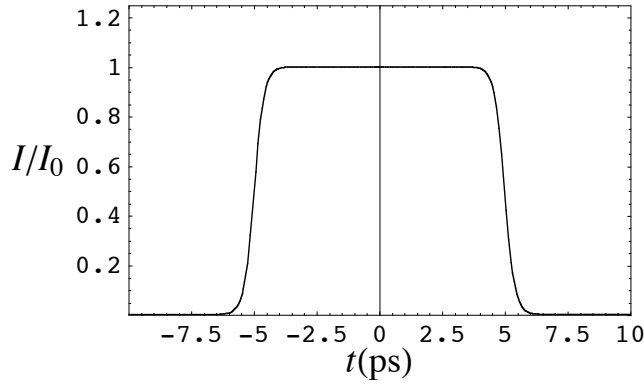
■ **Fitting Function for the Autocorrelation Curve: Square Pulse**

In general one is interested in extracting from the intensity interferogram of an SHG autocorrelation scan a measure of the laser pulse length. The relationship between the FWHM of the interferogram and the FWHM of the incident laser pulse depends upon the shape of the pulse. By assuming a Lorentzian pulse, for example, the relationship is a factor of two difference, with the laser pulse being shorter than the interferogram by a factor of 2. For the drive laser at Neptune we wish to obtain a realistic model for the shape of the laser pulse and derive from this the expected relationship between the FWHM of the pulse and the FWHM of the autocorrelation.

Let us take the laser pulse shape to be approximated by a square pulse with rounded edges. This type of pulse can be represented by a function of the following form:

$$I(t) = I_0 \frac{e^{-\alpha(t-\Delta t/2)}}{1 + e^{-\alpha(x-\Delta t/2)/T}} \frac{e^{\alpha(t+\Delta t/2)}}{1 + e^{\alpha(x+\Delta t/2)}} \quad (45)$$

where Δt is the FWHM of the pulse and $\alpha = \Delta t/T$ where T is the falloff time of the round edges. In the limit $T \rightarrow 0$, $\alpha \rightarrow \infty$ and the plot looks like a perfect square pulse of width Δt . We plot below an example, for the case $\Delta t = 10$ ps with a falloff time of $T = 2$ ps or $\alpha = 5$ ps⁻¹:



The autocorrelation function of this we will call $F(\tau)$ which we define by

$$F(\tau) = \int_{-\infty}^{\infty} I(t) I(t - \tau) dt \quad (46)$$

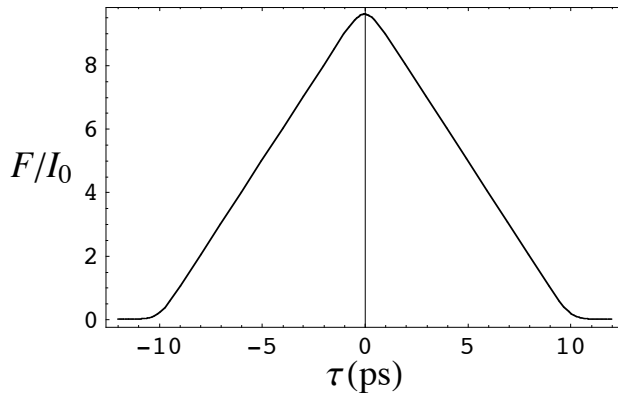
Equation (45) may be rewritten as

$$I(t) = I_0 e^{-\mu \Delta t} \frac{e^{-\mu(t-\Delta t/2)}}{1 + e^{-\mu(x-\Delta t/2)/T}} \frac{e^{\mu(t+\Delta t/2)}}{1 + e^{\mu(x+\Delta t/2)}} \quad (47)$$

where $\mu = -\alpha$. Then, μ is inherently negative and real. If one plots (47) with $\mu = -5$ ps⁻¹ and $\Delta t = 10$ ps the result exactly resembles the plot above. Inserting (47) into (46) and evaluating the integral, we obtain

$$F(\tau) = I_0 e^{-2\mu \Delta t} \frac{e^{\mu(2\Delta t + \tau)} \left((1 + e^{2\mu \Delta t}) (-1 + e^{\mu \tau}) \text{Log} \left[e^{\frac{\Delta t \mu}{2}} \right] + (e^{\mu \tau} - e^{2\mu \Delta t}) \text{Log} \left[e^{\mu \left(\frac{\Delta t}{2} + \tau \right)} \right] + (e^{\mu(\Delta t + \tau)} - 1) \left(\text{Log} \left[1 + e^{\mu \left(\frac{\Delta t}{2} - \tau \right)} \right] - \text{Log} \left[1 + e^{\mu \left(\tau - \frac{\Delta t}{2} \right)} \right] \right) \right)}{(1 - e^{2\mu \Delta t}) (e^{2\mu \Delta t} - e^{\mu \tau}) (e^{\mu \tau} - 1) (e^{\mu(\Delta t + \tau)} - 1) \mu}$$

Plotting this function for the example values used above, we obtain



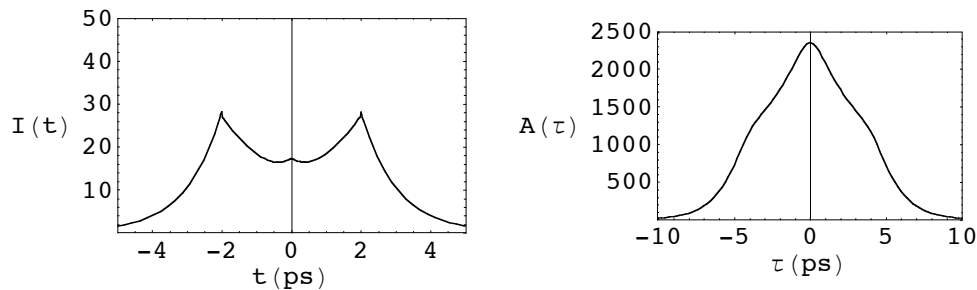
Evaluating $F(\tau)$ at $\tau = 0$ gives an indeterminate result since both the numerator and denominator vanish. However, evaluating by integrating (46) with $\tau = 0$ we obtain

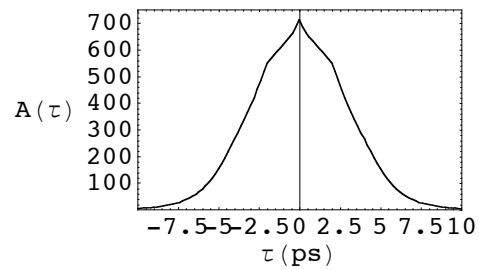
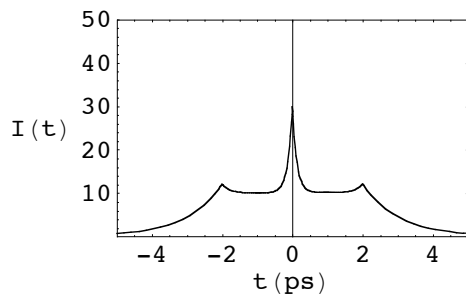
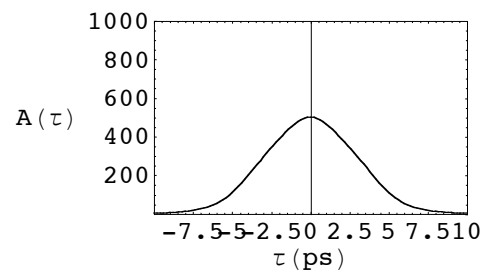
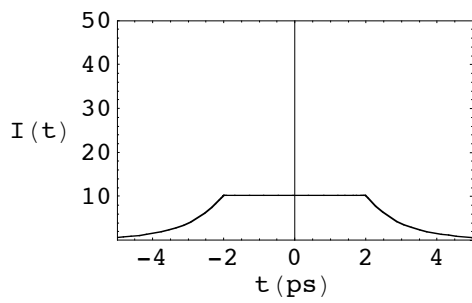
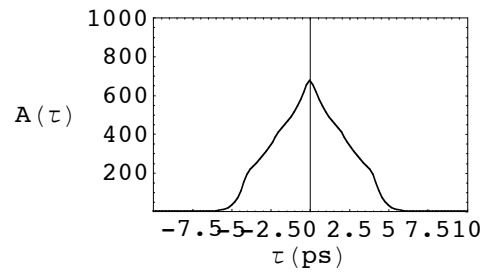
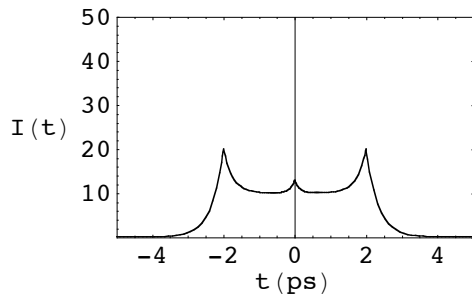
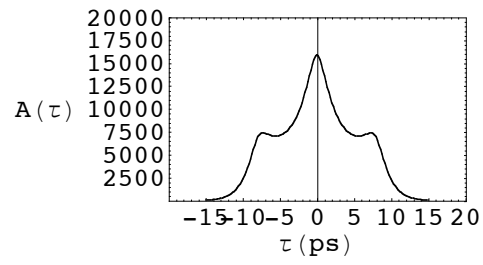
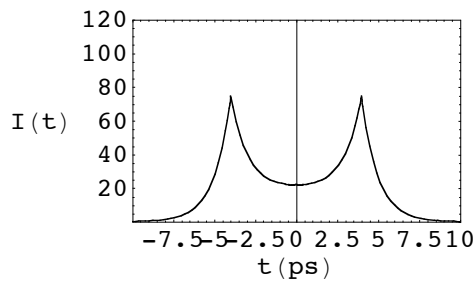
$$F_{\max} = \int_{-\infty}^{\infty} I(t)^2 dt = 2 I_0 \frac{e^{\Delta t \mu} + (1 + e^{\Delta t \mu}) \text{Log}\left[e^{-\frac{\Delta t \mu}{2}}\right] - 1}{(-1 + e^{\Delta t \mu})^3 \mu} \quad (49)$$

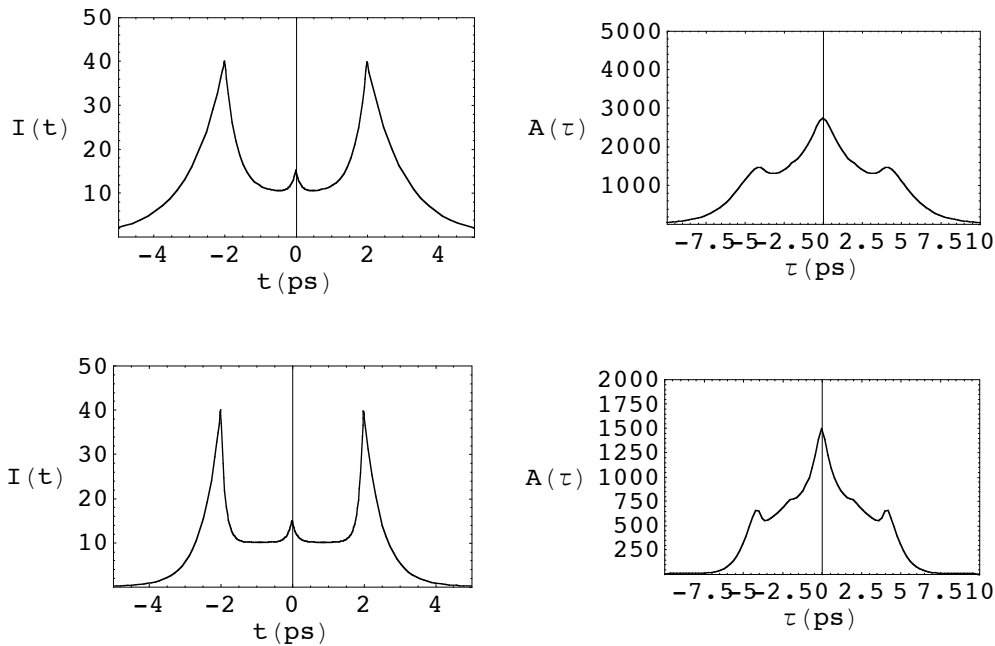
Evaluating this for the plot above, we obtain $F_{\max} / I_0 = 9.6$. Now we wish to find an expression for the FWHM of the function $F(\tau)$. This is done by solving the equation $F(\tau) = F_{\max} / 2$ for τ . However, this equation is too complicated to solve algebraically, so it must be done numerically. If the falloff at the edges of the square pulse is fairly short ($\alpha \rightarrow \infty$), we can see that the result will be that the full width half-max of the autocorrelation curve will be approximately $\text{FWHM} \approx \Delta t$.

■ Fitting Function for the Autocorrelation Curve: Square Pulse with Spikes

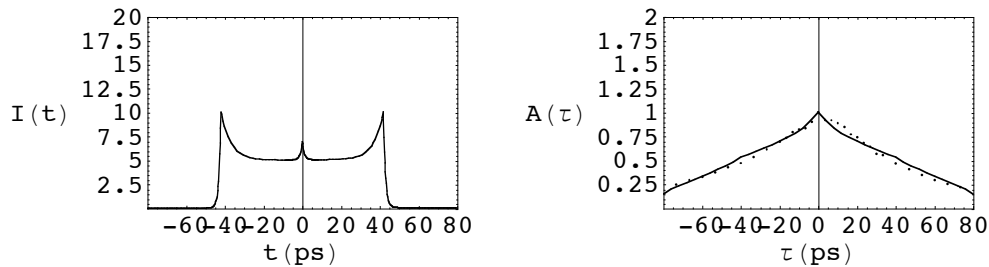
As the exact pulse shape of a laser pulse cannot be completely known from examination of the autocorrelation traces, various hypotheses exist about what type of pulse shape should be fitted to the data. One such hypothesis is that if one assumes an undercompressed final pulse with a remnant linear chirp, then there should be a direct relationship between the shape of the pulse and the shape of its power spectrum in the frequency domain. The power spectrum of the beam at the Neptune laboratory has a shape characterized by a square pulse with "spikes" on the edges, and some of the autocorrelation traces which have been observed are consistent with a pulse having this sort of time structure. Below are a variety of pulse intensity profiles $I(t)$ of this type and the resulting autocorrelation functions $A(\tau)$ which they would produce.





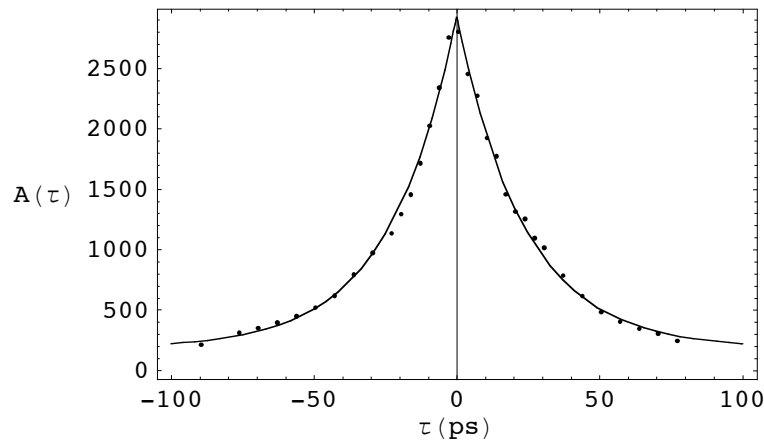


The following plot shows an example of a trial pulse shape which fits fairly closely to the observed autocorrelation data. The autocorrelation function in the second plot (solid curve) is superimposed with the actual data (dots).



■ **Fitting Function for the Autocorrelation Curve: Exponential Pulse**

As of this writing, data taken at the Neptune laboratory show that when the cathode drive laser is fully compressed, its autocorrelation function resembles an exponential mirrored about the vertical axis. Below is an example of autocorrelation data which are superimposed with an exponential fit function.



The fit function in this case has the form

$$A(\tau) = c + a e^{b|\tau|} ; \tag{50}$$

This sort of autocorrelation function can be produced by a time profile $I(t)$ which looks like an exponential function with a sharp cutoff (see the third example in the figure below). The following are examples of various asymmetric exponentials (on the left) and the autocorrelation functions $A(\tau)$ (on the right) which they produce.

